and of some conducting polymers. These findings open up tremendous possibilities for exploiting the highly designable visible and infrared optical properties of quantum dots of various shapes and compositions, along with the useful conductivity.

References and Notes

1. C. P. Collier, R. J. Saykally, J. J. Shiang, S. E. Henrichs, J. R. Heath, *Science* **277**, 1978 (1997).
2. S. H. Sun, C. B. Murray, D. Weller, L. Folks, A. Moser, *Science* **287**, 1989 (2000).
3. M. L. Steigerwald, L. E. Brus, *Acc. Chem. Res.* **23**, 183 (1990).
4. N. C. Greenham, X. G. Peng, A. P. Alivisatos, *Phys. Rev. B* **54**, 17628 (1996).
5. V. L. Colvin, M. C. Schlamp, A. P. Alivisatos, *Nature* **370**, 354 (1994).
6. C. Wang, M. Shim, P. Guyot-Sionnest, *Science* **291**, 2390 (2001).
7. C. B. Murray, C. R. Kagan, M. G. Bawendi, *Annu. Rev. Mater. Sci.* **30**, 545 (2000).
8. M. Drndic, M. V. Jarosz, N. Y. Morgan, M. A. Kastner, M. G. Bawendi, *J. Appl. Phys.* **92**, 7498 (2002).
9. C. A. Leatherdale *et al.*, *Phys. Rev. B* **62**, 2669 (2000).
10. D. S. Ginger, N. C. Greenham, *J. Appl. Phys.* **87**, 1361 (2000).
11. B. Enright, D. Fitzmaurice, *J. Phys. Chem.* **100**, 1027 (1996).
12. V. Noack, H. Weller, A. Eychmüller, *J. Phys. Chem. B* **106**, 8514 (2002).
13. B. O'Regan, M. Grätzel, *Nature* **353**, 737 (1991).
14. A. L. Roest, J. J. Kelly, D. Vanmaekelbergh, *Phys. Rev. Lett.* **89**, 036801 (2002).
15. C. K. Chiang *et al.*, *J. Am. Chem. Soc.* **100**, 1013 (1978).
16. R. C. Haddon *et al.*, *Nature* **350**, 320 (1991).
17. M. Shim, P. Guyot-Sionnest, *Nature* **407**, 981 (2000).
18. Materials and methods are available as supporting material on *Science* Online.
19. P. Guyot-Sionnest, M. A. Hines, *Appl. Phys. Lett.* **72**, 686 (1998).
20. R. Parthasarathy, X. M. Lin, H. M. Jaeger, *Phys. Rev. Lett.* **87**, 186807 (2001).
21. R. C. Doty, H. B. Yu, C. K. Shih, B. A. Korgel, *J. Phys. Chem. B* **105**, 8291 (2001).
22. K. C. Beverly, J. F. Sampaio, J. R. Heath, *J. Phys. Chem. B* **106**, 2131 (2002).
23. C. Wang, M. Shim, P. Guyot-Sionnest, *Appl. Phys. Lett.* **80**, 4 (2002).
24. P. Guyot-Sionnnest, C. Wang, *J. Phys. Chem. B*, 10.1021/jp0275084 (2003).
25. The differential mobility is determined as $\mu = 10^{-2}(w/L)(\partial G/\partial Q)$ where w is the 5-μm gap between electrodes, L is the 5-mm length of the electrode, and the 10^{-2} factor accounts for the 50 pairs of electrodes.
26. D. J. Norris, M. G. Bawendi, *Phys. Rev. B* **53**, 16388 (1996).

27. We thank M. Shim and T. Downes for their earlier exploratory work on alkali metal doping in our laboratory. D.Y. was supported by the University of Chicago–Argonne National Laboratory Consortium for Nanoscience Research. C.W. was supported by the U.S. National Science Foundation (NSF) under grant DMR-0108101. Use of the MRSEC Shared Facilities was supported by NSF under grant DMR-0213745.

Supporting Online Material

www.sciencemag.org/cgi/content/full/300/5623/1277/DC1

Materials and Methods

Figs. S1 and S2

12 March 2003; accepted 14 April 2003

Influence of Satellite Data Uncertainties on the Detection of Externally Forced Climate Change

B. D. Santer,[1]* T. M. L. Wigley,[2] G. A. Meehl,[2] M. F. Wehner,[3] C. Mears,[4] M. Schabel,[4] F. J. Wentz,[4] C. Ammann,[2] J. Arblaster,[2] T. Bettge,[2] W. M. Washington,[2] K. E. Taylor,[1] J. S. Boyle,[1] W. Brüggemann,[5] C. Doutriaux[1]

Two independent analyses of the same satellite-based radiative emissions data yield tropospheric temperature trends that differ by 0.1°C per decade over 1979 to 2001. The troposphere warms appreciably in one satellite data set, while the other data set shows little overall change. These satellite data uncertainties are important in studies seeking to identify human effects on climate. A model-predicted "fingerprint" of combined anthropogenic and natural effects is statistically detectable only in the satellite data set with a warming troposphere. Our findings show that claimed inconsistencies between model predictions and satellite tropospheric temperature data (and between the latter and surface data) may be an artifact of data uncertainties.

Since 1979, atmospheric microwave emissions have been monitored by the Microwave Sounding Unit (MSU) flown on polar-orbiting satellites (*1*). Satellite temperature measurements are mass-weighted averages of the microwave emissions from broad atmospheric layers (*2*). In the mid to upper troposphere, these emissions are monitored by MSU channel 2 ("T2"). Emissions from the stratosphere are tracked by MSU channel 4 ("T4").

The MSU record currently comprises measurements from 12 different satellites. Producing homogenous data sets requires accounting for such effects as intersatellite biases, uncertainties in instrument calibration coefficients, changes in instrument body temperature, drift in sampling of the diurnal cycle, roll biases, and decay of orbital altitude (*2–6*). Until recently, only one group (from the University of Alabama at Huntsville; hereafter, "UAH") had generated temperature records from the raw MSU radiative emissions data (*1*, *2*). On the basis of these records, it has been argued that the troposphere has not warmed over the satellite era, thus casting doubt on the usefulness of climate models (which predict that anthropogenic warming should have occurred), the reliability of thermometer-based observations of surface warming, and the reality of human-induced climate change (*7*).

A second group (Remote Sensing Systems in Santa Rosa, California; "RSS") has now constructed T2 and T4 temperature data sets from the same raw radiative emissions used by UAH (Fig. 1). Over 1979 to 2001, the global mean T2 temperatures estimated by the RSS group warm by roughly 0.1°C/decade relative to the corresponding UAH data, which show little net change (*6*).

Our goal was to explore the effects of this observational uncertainty on climate change detection results. We compared T2 and T4 temperatures from UAH and RSS with simulated MSU temperatures (*8*) from a climate change experiment performed with a state-of-the-art coupled atmosphere-ocean model, the Department of Energy Parallel Climate Model (PCM) developed by the National Center for Atmospheric Research and Los Alamos National Laboratory (*9*). The PCM experiment ("ALL") involves combined changes in well-mixed greenhouse gases, tropospheric and stratospheric ozone, the direct scattering radiative effects of sulfate and volcanic aerosols, and solar irradiance (*10*, *11*). Four realizations of ALL were performed, each with identical forcing but commencing from different initial conditions of the PCM control run. The experiments start in January 1890 and finish in December 1999.

We first show comparisons of global mean changes in ALL and observations. Both modeled and observed T4 data exhibit a multidecadal cooling trend (Fig. 1A), which is primarily attributable to stratospheric ozone depletion and to increases in well-mixed greenhouse gases (*12–14*). Only the RSS T4 trend of -0.44 ± 0.46°C/decade (the 95% confidence interval) is significantly different from zero at the 10% level (*15–17*) (Fig. 2A).

[1]Program for Climate Model Diagnosis and Intercomparison, Lawrence Livermore National Laboratory, Livermore, CA 94550, USA. [2]National Center for Atmospheric Research, Boulder, CO 80303, USA. [3]Lawrence Berkeley National Laboratory, Berkeley, CA 94720, USA. [4]Remote Sensing Systems, Santa Rosa, CA 95401, USA. [5]University of Birmingham, Edgbaston, Birmingham B15 2TT, UK.

*To whom correspondence should be addressed. E-mail: santer1@llnl.gov

Superimposed on this overall cooling are the stratospheric warming signatures of the El Chichón and Pinatubo volcanic eruptions, caused by increased absorption of incoming solar radiation and upwelling terrestrial infrared radiation by volcanic aerosols (*13*, *14*). Like other models, PCM overestimates this warming (*18*), largely due to coarse vertical resolution in the stratosphere.

The observed T2 data are characterized by large El Niño events in 1982–83 and 1997–98 (Fig. 1B). Fortuitously, one of the PCM realizations has an El Niño in 1996 with an amplitude comparable to that of the observed 1997–98 event (*19*). This is consistent with PCM's ability to simulate many of the statistical characteristics of El Niño–induced temperature variability (*20*). Another prominent feature of the observed T2 data is the cooling induced by Pinatubo. PCM's tropospheric temperature response to Pinatubo successfully captures the peak cooling, the time to reach this cooling, and the gradual recovery to pre-eruption temperature levels (*21*). Although the T2 cooling in response to El Chichón is clearly evident in PCM, it is masked in the observations by the 1982–83 El Niño (*19*).

RSS tropospheric temperatures warm by 0.10 ± 0.11°C/decade over 1979 to 1999, whereas the UAH T2 trend is close to zero (0.01 ± 0.11°C/decade) (Fig. 2B). T2 trends in the four ALL realizations lie within this observational range (*22*). If temporal autocorrelation effects are accounted for (*16*), only the RSS T2 trend is significantly different from zero at the 10% level (*23*). Different test outcomes are obtained if autocorrelation effects are neglected (fig. S1B). This highlights the importance of properly accounting for temporal autocorrelation in assessing the significance of individual trends and model-data trend consistency (*15*, *16*).

We next investigated whether observational uncertainty influences the outcome of model-data consistency tests that rely on full patterns of temperature change. We used a standard "fingerprinting" technique (*24*, *25*). The fingerprint $\vec{f}$ is assumed to be the first Empirical Orthogonal Function (EOF) of the ALL ensemble mean, and therefore represents the expected climate change signal in response to a suite of anthropogenic and natural forcings. Fingerprint detection requires estimates of the internally generated climate noise for assessing statistical significance. Here, we obtained noise estimates from 300-year control runs (with no external forcings) performed with two models: PCM, and the ECHAM4/OPYC model ("ECHAM") of the Max-Planck Institute for Meteorology in Hamburg (*26*).

Our strategy was to search for an increasing expression of $\vec{f}$ in the UAH and RSS data and to estimate the "detection time"—the time at which the fingerprint becomes consistently identifiable at a stipulated 5% significance level. We tried to enhance the detectability of $\vec{f}$ by rotating the fingerprint away from high noise components, yielding the optimized fingerprint $\vec{f}^*$. Given the short observational record lengths, we used only the spatial properties of signal and noise in rotating $\vec{f}$. Other detection efforts involving longer data sets with more temporal structure have employed both spatial and temporal information for fingerprint optimization (*27*, *28*).

For surface temperature, several studies have identified an anthropogenic fingerprint even after removal of global mean changes (*29*, *30*). Such "mean-removed" model-data pattern comparisons, which focus on subglobal spatial scales, provide more compelling statistical evidence of fingerprint detection than global mean agreement alone. We address this issue by performing our detection analysis both with and without the global mean changes in T2 and T4 temperatures. The "mean-included" fingerprints have uniform sign and pronounced zonal structures. For T4, the externally forced signal is largest poleward of 60°S (Fig. 3A). Highest loadings for the T2 fingerprint are in the tropics (Fig. 3C). Removal of the spatial means emphasizes the strong equator-to-pole gradients and zonal structure in both the T4 and T2 fingerprints (Fig. 3, B and D).

Detection times are shown in Fig. 4. For each variable (T2 or T4), there are eight mean-included and eight mean-removed cases. Each group of eight is comprised of four nonoptimized (RAW) and four optimized (OPT) results. We considered the T4 detection times first. Without optimization, the mean-included fingerprint is identifiable in both observational data sets in 1988, only 10 years after the start of the satellite record (Fig. 4A). This early detection arises from increasing similarity between the fingerprint and the spatially coherent pattern of stratospheric cooling common to UAH and RSS (Fig. 3A and Fig. 5, A and C). Such increases in pattern similarity cannot be obtained using simulated natural internal variability alone.

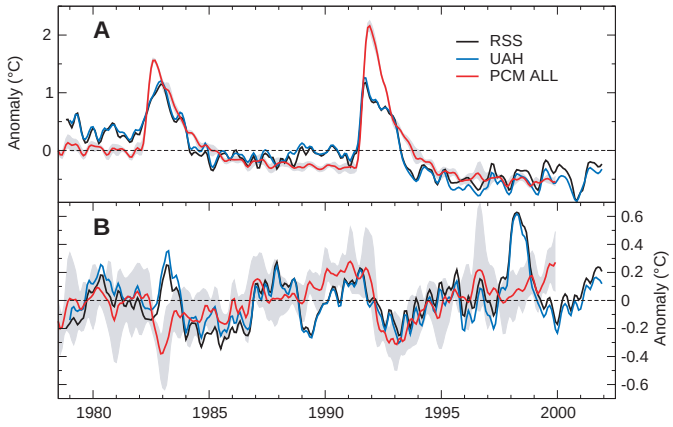

Fig. 1. Time series of observed and simulated monthly mean, spatially averaged MSU temperature anomalies for (**A**) the stratosphere (T4) and (**B**) mid to upper troposphere (T2). Observations are from UAH (*2*) and RSS (*6*). Simulated MSU temperatures are the ensemble mean of four different realizations of a PCM model experiment with combined natural and anthropogenic forcing (*9*). The gray shaded areas define the range between the highest and lowest values of the realizations. All data are expressed as anomalies relative to climatological monthly means over 1979 to 1999 and were low-pass filtered. The ALL experiment ends in December 1999, whereas UAH and RSS data used here end in December 2001.

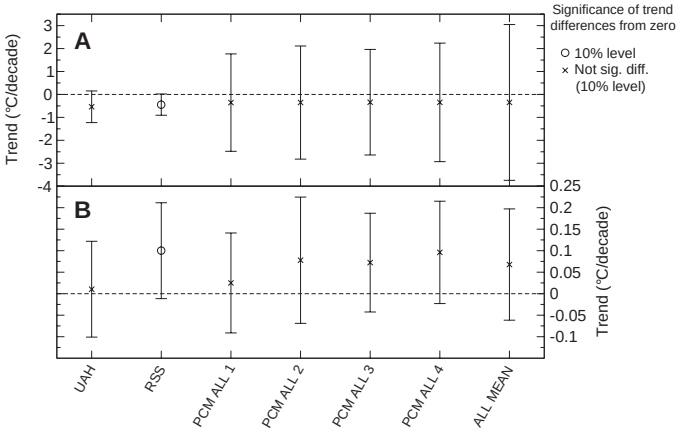

Fig. 2. Comparison of individual observed (UAH, RSS) and simulated (PCM) temperature trends over January 1979 through December 1999, the period of overlap between the UAH and RSS data and the ALL experiment. Results are for (**A**) T4 and (**B**) T2. Model trends are shown for individual ALL realizations and the ALL ensemble mean. Error bars indicate the 95% confidence intervals, adjusted for temporal autocorrelation effects (*15*, *16*). Different symbol types provide information on whether individual trends are significantly different from zero (*16*). Trends were computed from the monthly mean anomaly data in Fig. 1.

Positive detection of the nonoptimized T4 fingerprint is not driven solely by global mean behavior. Removal of spatial mean changes still yields a detectable RAW fingerprint, but only toward the end of the record (between 1997 and 2001) (Fig. 4A). In this case, detection is due to model-data similarities in both the equator-to-pole temperature gradient and the hemispheric asymmetry of stratospheric temperature changes. In terms of the latter, both the RAW T4 fingerprint and the UAH and RSS data have larger high-latitude cooling in the Southern Hemisphere than in the Northern Hemisphere (Fig. 3B and Fig. 5, A and C). Systematic differences in the latitudinal structure of the observed cooling (Fig. 5E) probably explain why the RAW mean-removed fingerprint has slightly different detection times in the RSS and UAH data.

In our approach, 1988 is the earliest time at which fingerprint detection can occur. Because the RAW mean-included T4 fingerprint is already detectable in 1988, optimization of $\vec{f}$ cannot improve this result (Fig. 4A). When the spatial mean is removed, however, optimization markedly advances RAW detection times. For example, optimization transforms "late" detection of $\vec{f}$ (between 1997 and 2001) to "early" detection of $\vec{f}$* (in 1988).

The detectability of tropospheric temperature change fingerprints shows greater dependence on the choice of observational data set. In the mean-included case, the RAW and OPT T2 fingerprints are consistently identifiable in RSS data, but not in UAH (Fig. 4B). This difference in detectability is primarily due to RSS-UAH differences in global mean trends (Fig. 2B). In contrast, the mean-removed T2 fingerprint is detectable at the 5% level in both observational data sets (in 6 of 8 cases) (Fig. 4B). This result reflects the pronounced equator-to-pole temperature gradients common to $\vec{f}$ and the observations (Fig. 3D and Fig. 5, B and D). These gradients are preserved after removal of spatial means. As for T4, latitudinal differences in the two observed data sets (Fig. 5F) lead to slightly different mean-removed detection times. Both T4 and T2 results show some sensitivity to the choice of noise data, with detection often achieved later if ECHAM noise is used for testing statistical significance.

The satellite data uncertainties presented here arise from different processing choices made by the UAH and RSS groups. For T2 data, UAH-RSS discrepancies are primarily related to how the two groups deal with the "instrument body effect" (IBE), and how they account for satellite drift in sampling the diurnal temperature cycle. The IBE arises from correlations between the MSU-measured brightness temperature and the temperature of the hot calibration target for the MSU instrument (*2*, *6*). A "target factor" quantifies this correlation. RSS and UAH arrive at different estimates of this factor, particularly for channel 2 of the MSU instrument on the NOAA-9 satellite. In this case, the UAH-estimated target factor is substantially larger than the RSS target factor and the target factors of any other MSU instruments or channels (*6*).

Our analysis shows that PCM's T2 changes are generally in better agreement with RSS than with UAH. Other models yield qualitatively similar results. Though simulated T2 changes in climate models run with similar forcings are larger than in PCM or either observational data set, they are still closer to RSS than to UAH (*14*, *31*). We cannot use model-data comparisons alone, however, to determine which of the two satellite data sets is closer to reality. One reason for this is that the estimated historical forcing used in climate model experiments does not include all possible anthropogenic influences (*32*). A key forcing neglected in the present work, for example, is that arising from indirect aerosol effects. Repetition of our detection study with ECHAM fingerprints that include this forcing does not alter the primary conclusions of this paper (*33*).

Consistency with observed surface temperature changes is another factor that may be useful in evaluating the reliability of the RSS and UAH MSU data. Observations of a strongly warming surface are in better accord with T2 changes in RSS than in UAH (*21*). Comparisons with surface data

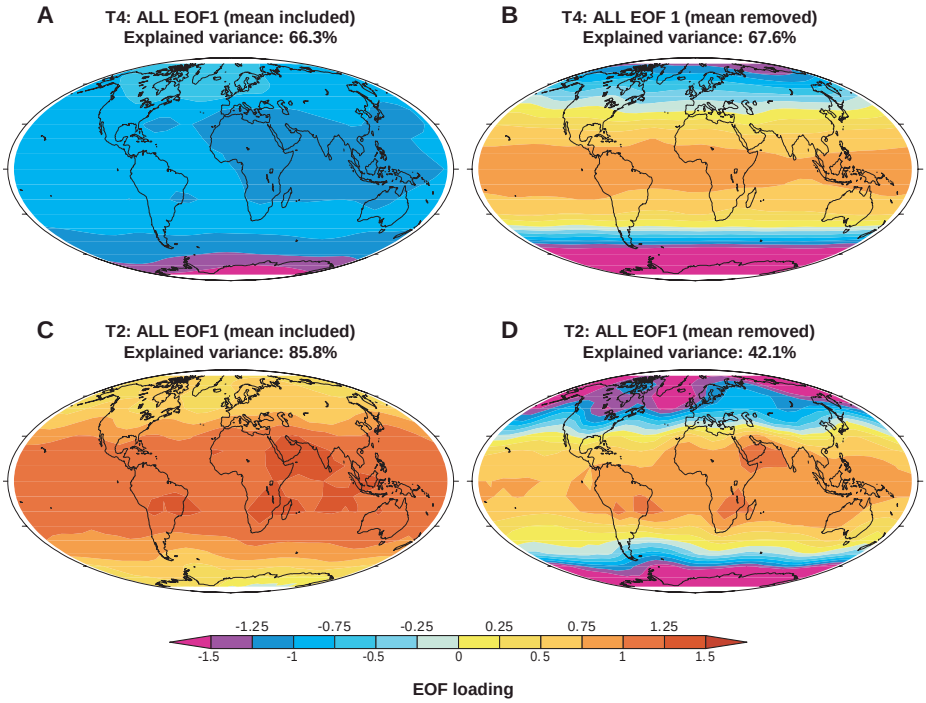

Fig. 3. RAW climate change "fingerprint" patterns for (**A** and **B**) T4 and (**C** and **D**) T2 data from the PCM ALL experiment. Results are shown for analyses with the spatial mean included (A) and (C) and with the mean removed (B) and (D).

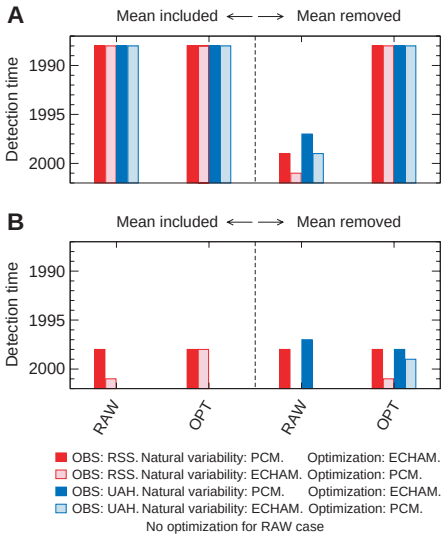

Fig. 4. Detection times for PCM (**A**) T4 and (**B**) T2 temperature change fingerprints in RSS and UAH observational data. The detection analysis uses both the mean-included and mean-removed fingerprints from Fig. 3, with a 5% significance level as the detection threshold (*25*). The longer the colored bar, the earlier the detection time. If no bar is present, fingerprints could not be identified before the final year (2001) of the observations. RAW and OPT denote detection times for nonoptimized and optimized fingerprints, respectively. To avoid the introduction of artificial skill (*27*), the model control run used for optimization was always different from the control run used for estimating natural variability statistics.

must be treated cautiously, in part because T2 has a small (roughly 10%) contribution from the cooling stratosphere. Radiosonde temperature measurements afford another means of judging the quality of satellite data (*2*, *3*). As with MSU data, however, there is evidence that the choice of the "adjustment pathway" for radiosonde data markedly influences the size and even the sign of the estimated global-scale trend (*34*). Furthermore, many of the largest differences between RSS and UAH T2 trends are in areas where radiosonde coverage is sparse.

Although the RSS T2 data are more consistent with both model results and surface observations, we cannot say definitively whether RSS or UAH provides a better estimate of the "true" tropospheric temperature changes. This dilemma may be resolved by analysis of complementary data sets, such as tropopause height, water vapor, and sea-surface temperature (SST) (*18*, *35*). Better characterization of the diurnal cycle in satellite data correction procedures would also help to reduce UAH-RSS differences.

In summary, we note two important points. First, claimed inconsistencies between satellite estimates of tropospheric temperature changes and either model results or surface temperature trends depend critically on which satellite data set is used. These inconsistencies are minimized with the RSS data. Second, our identification of a model-predicted stratospheric temperature fingerprint is robust to satellite data uncertainties. Taken together, these points strengthen the case for a pronounced human influence on global climate (*36*).

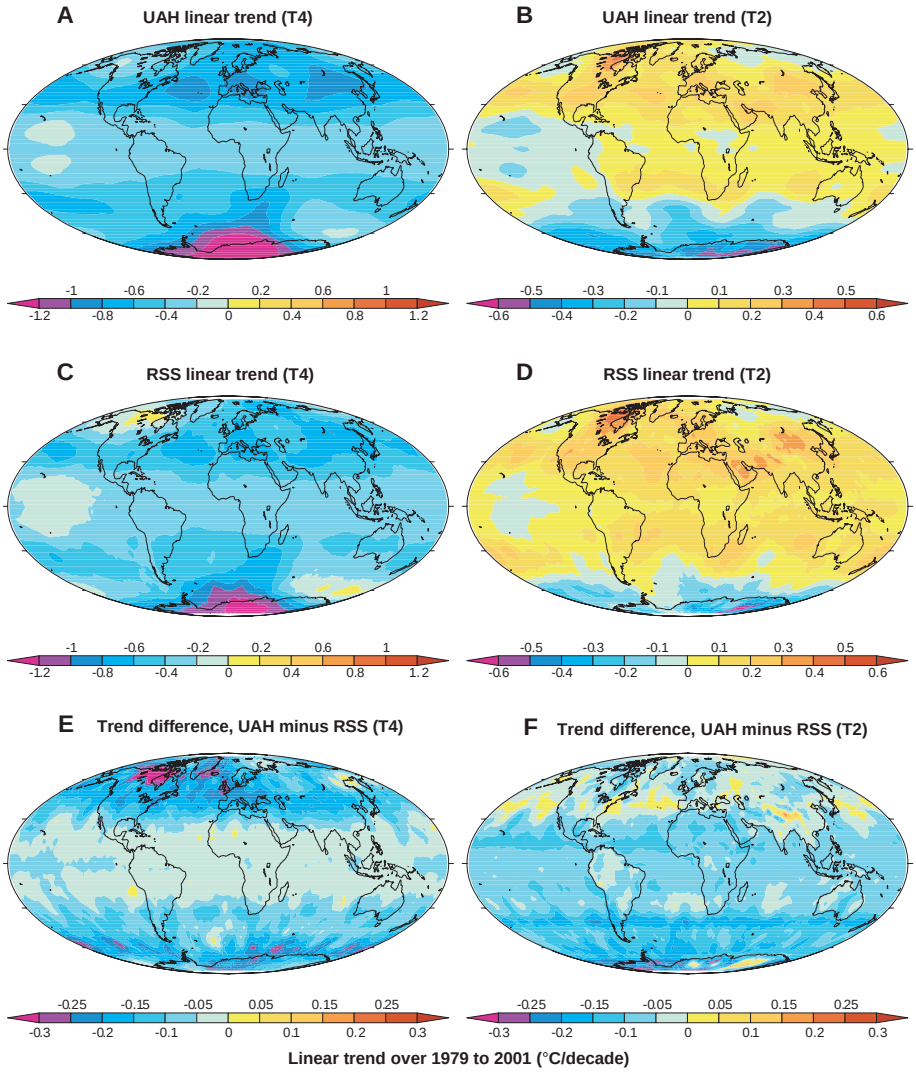

Fig. 5. Linear trends (*16*) over January 1979 to December 2001 in the UAH and RSS T4 and T2 data, computed from anomalies defined relative to overall climatological monthly means. T4 results for UAH and RSS are in (**A**) and (**B**); T2 results for the same are in (**C**) and (**D**), respectively. The spatial patterns of differences between the UAH and RSS trend fields are given in (**E**) and (**F**) for the T4 and T2 data, respectively.

References and Notes

1. R. W. Spencer, J. R. Christy, *J. Clim.* **5**, 847 (1992).
2. J. R. Christy, R. W. Spencer, W. D. Braswell, *J. Atmos. Ocean. Tech.* **17**, 1153 (2000).
3. J. M. Wallace *et al.*, *Reconciling Observations of Global Temperature Change* (National Academy Press, Washington, DC, 2000).
4. F. J. Wentz, M. Schabel, *Nature* **394**, 661 (1998).
5. J. W. Hurrell, K. E. Trenberth, *Nature* **386**, 164 (1997).
6. C. A. Mears, M. C. Schabel, F. W. Wentz, in preparation.
7. S. F. Singer, *EOS* **80**, 183 (1999).
8. B. D. Santer *et al.*, *J. Geophys. Res.* **104**, 6305 (1999).
9. W. M. Washington *et al.*, *Clim. Dyn.* **16**, 755 (2000).
10. C. Ammann, G. A. Meehl, W. M. Washington, C. Zender, *Geophys. Res. Lett.* **30**, doi: 10.1029/2003GL016875RR.
11. G. A. Meehl, W. M. Washington, T. M. L. Wigley, J. M. Arblaster, A. Dai, *J. Clim.*, **16**, 426 (2003).
12. V. Ramaswamy, M. D. Schwarzkopf, W. Randel, *Nature* **382**, 616 (1996).
13. V. Ramaswamy *et al.*, *Rev. Geophys.* **39**, 71 (2001).
14. J. E. Hansen *et al.*, *J. Geophys. Res.* **107**, doi: 10.1029/2001JD001143 (2002).
15. B. D. Santer *et al.*, *J. Geophys. Res.* **105**, 7337 (2000).
16. These are the "adjusted" 95% confidence intervals for b, the slope parameter of the estimated least-squares linear trend (*15*). Our adjustment procedure assumes a lag-1 temporal autocorrelation structure of the trend residuals, $e(t)$. The lag-1 autocorrelation coefficient of $e(t)$ is used to compute an effective sample size, n_e, and to adjust s_b, the standard error of b. Strong temporal autocorrelation of $e(t)$ results in $n_e \ll n$ (the actual number of time samples) and inflates s_b. Tests of the significance of b involve the ratio b/s_b, which is assumed to be distributed as Student's t. Some studies have assumed (incorrectly) that values of $e(t)$ are statistically independent, thus biasing estimates of s_b and trend significance. We show both adjusted and unadjusted results (Fig. 2 and fig. S1, respectively) to illustrate the dependence of trend significance estimates on test assumptions. All significance estimates involve a conservative two-tailed Student's t test of the null hypothesis that b is not significantly different from zero. For adjusted results, n_e is used for calculating s_b and determining the critical t value. Unadjusted results use n instead of n_e.
17. For T4, adjusted confidence intervals are much smaller in observations than in the four ALL realizations (Fig. 2A), primarily due to PCM's overestimate of the stratospheric temperature responses to El Chichón and Pinatubo (Fig. 1A). Note that ensemble averaging reduces internally generated noise and increases the autocorrelation of trend residuals. This is why adjusted confidence intervals in the "ALL MEAN" case are not smaller than in individual ALL realizations (Fig. 2A).
18. B. D. Santer *et al.*, *J. Geophys. Res.* **108**, doi: 10.1029/2002JD002258 (2003).
19. The precise timing of El Niño and La Niña events (and hence of their effects on tropospheric temperatures) is not the same in the PCM simulations and in the real world. Similar timing of modeled and observed El Niño variability occurs in integrations with an atmospheric general circulation model (GCM) driven by observed changes in SST (*21*). Such similarities do not occur (except by chance) in a coupled atmosphere-ocean GCM like PCM.
20. G. A. Meehl *et al.*, *Clim. Dyn.* **17**, 515 (2001).
21. B. D. Santer *et al.*, *J. Geophys. Res.* **106**, 28033 (2001).
22. The fact that the PCM T2 results fall within the UAH and RSS range is unlikely to be due to compensating errors in PCM, such as excessive stratospheric cooling offsetting unrealistically large upper tropospheric warming. PCM's stratospheric cooling is smaller than in either UAH or RSS, which rules out error compensation (at least at the global mean level) as a plausible explanation for model-data trend correspondence.
23. None of the model trends is significantly different from the observed T2 trends (at the 10% level or better).
24. K. Hasselmann, in *Meteorology of Tropical Oceans*,

D. B. Shaw, Ed., (Royal Meteorological Society of London, London, 1979), pp. 251–259.
25. B. D. Santer *et al.*, *J. Geophys. Res.* **100**, 10693 (1995).
26. E. Roeckner, L. Bengtsson, J. Feichter, J. Lelieveld, H. Rodhe, *J. Clim.* **12**, 3004 (1999).
27. M. R. Allen, S. F. B. Tett, *Clim. Dyn.* **15**, 419 (1999).
28. P. A. Stott *et al.*, *Science* **290**, 2133 (2000).
29. G. C. Hegerl *et al.*, *J. Clim.* **9**, 2281 (1996).
30. P. A. Stott, S. F. B. Tett, *J. Clim.* **11**, 3282 (1998).
31. S. F. B. Tett *et al.*, *J. Geophys. Res.* **107**, doi 10.1029/2000JD000028 (2002).
32. V. Ramaswamy *et al.*, in *Climate Change 2001: The Scientific Basis*, J. T. Houghton *et al.*, Eds. (Cambridge Univ. Press, Cambridge, 2001), pp. 349–416.
33. The PCM climate change experiments available to us did not consider indirect aerosol forcing. However, we did have access to an ECHAM experiment that incorporated the indirect effects of anthropogenic sulfate aerosols on cloud albedo (*26*). Like the PCM ALL experiment, the ECHAM integration (GSDIO) applied changes in well-mixed greenhouse gases, sulfate aerosol direct effects, and tropospheric ozone. GSDIO differed from ALL both in its inclusion of indirect sulfate aerosol effects and in its neglect of changes in solar irradiance, volcanic aerosols, and stratospheric ozone. These differences in the ALL and GSDIO forcings (and the fact that no ECHAM experiment included all GSDIO forcings except indirect sulfate aerosols) make it difficult to isolate the influence of indirect sulfate aerosols on the detection of T4 and T2 fingerprints. Nevertheless, we note that repeating our detection analysis with GSDIO fingerprints yields results qualitatively similar to those obtained with PCM (fig. S2 and Fig. 4, respectively). This suggests that our primary conclusions may be relatively insensitive to the inclusion of indirect sulfate aerosol effects. The main difference between the PCM and ECHAM results is the delayed and less robust detection of the GSDIO mean-removed T4 fingerprint, which is probably due to GSDIO's neglect of stratospheric ozone depletion. Another difference is that the GSDIO mean-removed T2 fingerprint is detected earlier and more consistently than the corresponding PCM ALL fingerprint.
34. J. R. Lanzante, S. A. Klein, D. J. Seidel, *J. Clim.* **16**, 241 (2003).
35. F. J. Wentz, M. Schabel, *Nature* **403**, 414 (2000).
36. J. F. B. Mitchell *et al.*, in *Climate Change 2001: The Scientific Basis*, J. T. Houghton *et al.*, Eds. (Cambridge Univ. Press, Cambridge, 2001), pp. 695–738.
37. Work at Lawrence Livermore National Laboratory (LLNL) was performed under the auspices of the U.S. Department of Energy (DOE), Environmental Sciences Division, contract W-7405-ENG-48. T.M.L.W. was supported by the National Oceanic and Atmospheric Administration Office of Global Programs ("Climate Change Data and Detection") grant no. NA87GP0105, and by DOE grant no. DE-FG02-98ER62601. A portion of this study was supported by the DOE Office of Biological and Environmental Research, as part of its Climate Change Prediction Program. The MSU T2 and T4 data and static MSU weighting functions were provided by J. Christy (Univ. of Alabama in Huntsville). ECHAM model data were supplied by E. Roeckner. We thank T. Barnett and an anonymous reviewer for useful comments and suggestions.

Supporting Online Material
www.sciencemag.org/cgi/content/full/1082393/DC1
SOM Text
Figs. S1 and S2

15 January 2003; accepted 23 April 2003
Published online 1 May 2003;
10.1126/science.1082393
Include this information when citing this paper.

A Modular PIP_2 Binding Site as a Determinant of Capsaicin Receptor Sensitivity

Elizabeth D. Prescott and David Julius*

The capsaicin receptor (TRPV1), a heat-activated ion channel of the pain pathway, is sensitized by phosphatidylinositol-4,5-bisphosphate (PIP_2) hydrolysis after phospholipase C activation. We identify a site within the C-terminal domain of TRPV1 that is required for PIP_2-mediated inhibition of channel gating. Mutations that weaken PIP_2-TRPV1 interaction reduce thresholds for chemical or thermal stimuli, whereas TRPV1 channels in which this region is replaced with a lipid-binding domain from PIP_2-activated potassium channels remain inhibited by PIP_2. The PIP_2-interaction domain therefore serves as a critical determinant of thermal threshold and dynamic sensitivity range, tuning TRPV1, and thus the sensory neuron, to appropriately detect heat under normal or pathophysiological conditions.

Charged membrane phospholipids are thought to regulate a variety of ion channels and transporters (*1*). For example, recent electrophysiological studies suggest a role for the membrane phospholipid PIP_2 as a modulator of transient receptor potential (TRP) channels, many of which contribute to the detection of sensory stimuli. TRP channels in the *Drosophila* eye (*2*) and TRPV1 channels in the mammalian pain pathway (*3*, *4*) are activated or potentiated when PIP_2 is hydrolyzed, whereas the ubiquitously expressed mammalian TRPM7 channel is inhibited by PIP_2 cleavage (*5*). Phospholipase C (PLC) catalyzes the hydrolysis of PIP_2 to inositol trisphosphate (IP_3) and diacylglycerol (DAG) and has been implicated in the release of TRPV1 from PIP_2-mediated inhibition (*3*), although the underlying mechanism for such regulation has not been elucidated. Despite functional evidence that TRP channels are directly regulated by PIP_2, there is now no structural basis to account for this effect. TRPV1 is an especially tractable model for addressing this question, because it can be directly gated by a number of stimuli, including the pungent vanilloid compound capsaicin, extracellular protons (pH $<$ 6.0), or noxious heat ($>$43°C) (*6*, *7*). Moreover, genetic studies have shown that TRPV1 is an essential component of the signaling pathway through which PLC-coupled receptors increase behavioral sensitivity to heat (*3*, *8*, *9*), which makes elucidation of this regulatory pathway of physiological interest.

To investigate the molecular basis of PIP_2-dependent regulation, we determined which regions of TRPV1 were required for PLC-mediated potentiation. We reasoned that mutations affecting such domains should render TRPV1 insensitive to PIP_2 inhibition, and therefore, we identified mutants exhibiting increased responses to capsaicin or extracellular protons. A TRPV1 mutant lacking a segment of the C-terminal cytoplasmic domain (TRPV1 Δ777–820) produced much larger currents than wild-type channels in response to low doses of capsaicin (250 nM) or protons (pH 5.5), when expressed in *Xenopus* oocytes (Fig. 1). These enhanced currents could not be attributed to increased cell surface expression, because biotinylation experiments revealed equivalent levels of the mutant and wild-type TRPV1 at the plasma membrane (fig. S1). To determine whether amino acids 777 to 820 were also required for PLC-mediated potentiation, we exposed oocytes expressing TRPV1 channels and the nerve growth factor (NGF) receptor TrkA/p75 to NGF, a treatment that normally elicits a robust potentiation wild-type TRPV (~20-fold) of responses through activation of PLC-γ (*3*). Currents from TRPV1Δ777–820 were unchanged, which suggests that these residues are critical for mediating potentiation downstream of PLC-coupled receptor stimulation. Moreover, potentiation of TRPV1Δ777–820 was not observed when other PLC-coupled receptors were activated, including the epidermal growth factor receptor (EGFR) and the G protein–coupled m1 muscarinic acetylcholine receptor (*10*). Loss of potentiation was not simply due to increased agonist sensitivity of the mutant channel, because the response to either a low dose of capsaicin (100 nM) or protons (pH 6.1) was unchanged after PLC activation (*10*). In addition, the thermal threshold of TRPV1Δ777–820 was markedly shifted to lower temperatures, and the overall currents were larger than those of wild-type channels (Fig. 1D), a phenotype reminiscent of wild-type channels that have been potentiated by PLC-coupled receptor activation (*3*).

Department of Cellular and Molecular Pharmacology, University of California, San Francisco, CA 94143–2140, USA.

*To whom correspondence should be addressed. E-mail: julius@cmp.ucsf.edu